https://doi.org/10.1016/j.apacoust.2016.11.006

A numerical investigation on the sound insulation of ventilation windows

Xiang YU,[1)] Siu-Kit LAU,[2)] Li CHENG,[3)] Fangsen CUI[1)*]

1) Institute of High Performance Computing, A*STAR, Singapore, 138632

2) Department of Architecture, National University of Singapore, Singapore, 117566

3) Department of Mechanical Engineering, The Hong Kong Polytechnic University, Hong Kong, 90077

Abstract

A simulation model is proposed and developed for predicting the sound insulation performance of ventilation windows in buildings, which complies with the laboratory measurement standard ISO 10140. Finite element method (FEM) with verified model definitions is implemented to characterize the airborne sound transmission. An acoustic cavity with rigid-boundaries is used to simulate the diffuse field on the source side of the window, with its diffuseness verified with the pressure field uniformity. On the receiver side, a free field with an infinite baffle is assumed to capture the transmitted sound power. The Sound Reduction Index (SRI) is calculated from the difference between the source and receiving sound power levels in the one-third octave band. Using the proposed model, different ventilation window configurations, consisting of partially open single glazing, double glazing with staggered openings and that with sound absorbers are systematically investigated. Parametric studies are carried out to investigate the effects of various window dimensions and absorber parameters. Simple formulas are proposed for estimating the SRI in the mid-to-high frequency range, providing guidelines for engineering designs. The validity of the numerical model is confirmed by comparisons with full-scale experimental results.

Keywords: ventilation window, sound reduction index, diffuse field, finite element method, micro-perforated panel

1. Introduction

The need of environmental sustainability calls for the development of natural ventilation technologies to enhance occupant comfort for high-performance buildings. Traditionally, casement windows, top-hung windows and single sliders are commonly adopted window designs, whose structures are simply formed by a single layer of partially open glazing. However, the ventilation openings can easily cause poor noise insulation problem, hampering their uses in densely populated and noisy areas. Hence, the design of building windows capable of achieving natural ventilation whilst warranting required noise mitigation remains an attractive and challenging topic. In 1970s, Ford and Kerry [1, 2] first proposed the use of partially open double glazing with staggered inlet-outlet openings to improve the sound insulation. By conducting laboratory and field tests, they claimed the window could provide satisfactory acoustic and ventilation performance. Since then, this simple window construction has aroused continuous research interests [3-11]. For example, Kang *et al.* [3, 4] studied the feasibility of integrating transparent micro-perforated absorbers into the air channel between the double glazing. Through extensive experiments, they demonstrated the acoustic responses were sensitive to the selection of window parameters, showing the need for a prediction model. By adopting active noise cancellation technology, Huang *et al.* [5] further mitigated the low-frequency noise penetrating through the air channel. More recently, Sondergaard and Olesen [7, 8] prototyped a "supply air window" and attempted to optimize its acoustic performance. Tong *et al.* [9, 10] proposed a "plenum window" and conducted both scale-down laboratory and *in-situ* field

measurement. It was shown from these experimental works that open double glazing can significantly improve the sound insulation compared to open single glazing. With appropriate treatment of sound absorbing materials, the resultant SRI can even be comparable to a closed single glazing. Nevertheless, a numerical model that can systematically address the need for design and optimization is still lacking. This becomes increasingly important considering the large number of parameters involved in the system design, which, without a reliable simulation model, can hardly be entertained.

Theoretically, the Sound Reduction Index (SRI), as the basic measure of the sound insulation capability of a window, characterizes the proportion of incident sound energy that cannot transmit through its surface. To measure the SRI, ISO 10140 standards [12] specify the necessary requirements and practical guidelines for conducting the laboratory experiments. A schematic diagram of the test-rig is shown in Fig. 1, where the test specimen is mounted on a separation wall between a source and a receiving room. Although the test procedure has been well documented, the experiment is only useful for testing the performance of an existing window rather than for seeking a better design, mainly due to the cost of prototypes, experimental reliability and repeatability issues. To solve this problem and potentially shorten the product development cycle, many recent studies have attempted to develop numerical models facilitating the prediction of insulating structures [13-20]. For example, Papadopoulos [13, 14] used a virtual laboratory tool to calculate the wall Transmission Loss (TL), where an algorithm was proposed to optimize the shape of

the test rooms to obtain adequate diffuseness. Chazot and Guyader [15] formularized a computationally efficient patch-mobility method to predict the TL of a double panel coupled with an air cavity. The simulation repeatability issue caused by the variation of room dimensions and source locations was discussed by Dijckmans and Vermeir [17]. Unfortunately, despite the numerous works found on closed structures, simulations on open windows are scarce, if not inexistent, to the best knowledge of the authors.

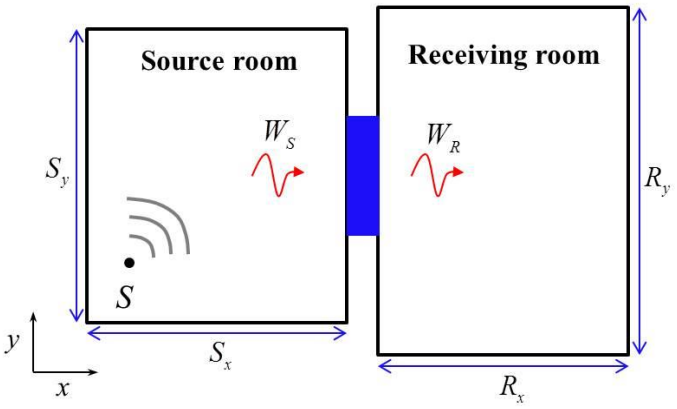

Fig. 1. Experimental evaluation of the SRI of a window, as specified by ISO 10140.

The aim of this study is to develop a numerical model for predicting the acoustic performance of open windows, with an attempt to systematically address the effect of changing window parameters. To comply with ISO standard, the source field is modeled as a large acoustic cavity with rigid boundaries, for simulating a diffuse room condition [21, 22]. The diffuseness is verified with the spatial uniformity of the pressure field within the domain using a proposed theoretical formulation. As for the radiation field on the receiver side, a free space with an infinite rigid baffle is assumed to capture the transmitted sound power, which mimics an anechoic chamber in the experiment [3, 15]. The sound power levels on the source and receiving side of the

window, characterized by the acoustic properties of the two fields, respectively, are obtained to calculate the SRI of the window in one-third (1/3) octave frequency band. Detailed descriptions of the proposed simulation model are presented in Sec. 2.

Based on the proposed numerical model, the SRI characteristics of typical ventilation window configurations will be investigated. An open single glazing is illustrated in Fig. 2 (a), where the opening refers to the area which is physically open, allowing for free air passage. In practical implementations, the window can operate either by sliding or pivoting to control the degree of the opening. Note that the two operating methods will not be distinguished in this study. Instead, the dominating effect of changing the opening size will be systematically investigated. Figures 2(b) & (c) illustrate two open double glazing configurations with rigid surfaces or with sound absorbers inside. The sound absorbing material shown in Fig. 2(c) uses a piece of transparent micro-perforated panel (MPP) with honeycomb backing cavity [23]. The real three-dimensional window (3D) configurations can be considered as simple extrusions from the two-dimensional (2D) cross-sections. By assuming the sound transmission is mainly determined by the opening size and the open cavity resonances in the longitudinal and vertical directions, 2D simulations only simulating a window cross-section are performed in Sec. 3. The effect of changing window geometries and adding sound absorbers will be systematically discussed. Finally, an experimental validation is carried out to validate the proposed numerical model, showing its effectiveness for practical designs.

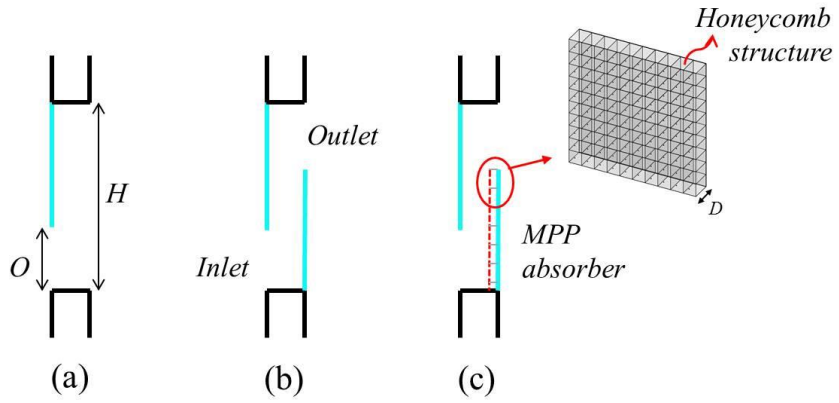

Fig. 2. (a) Open single glazing; (b) Open double glazing, the inlet-outlet openings are staggered; (c) Open double glazing with sound absorber, e.g., honeycomb MPP.

2. Simulation model

2.1 Diffuse source room

ISO 10140 suggests the use of a reverberant room to excite the test structure, so that the incident sound energy is uniformly distributed over the surface of the specimen [12]. This also enables the incident power to be characterized by averaging the sound intensity inside the source room. A large rigid-walled acoustic cavity is usually adopted. This section proposes a theoretical formulation to check whether an adequate diffuseness has established for the source room used in the simulation.

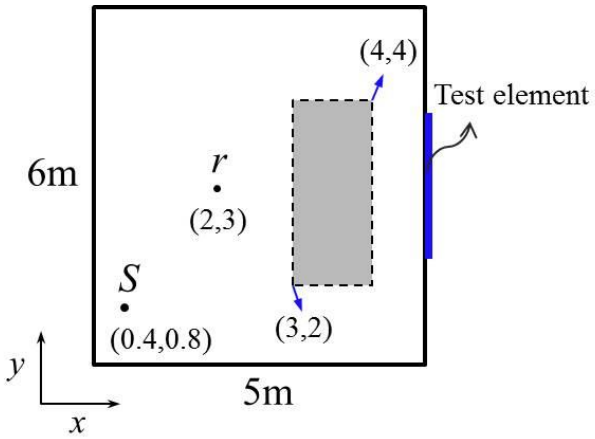

Fig. 3. A rectangular cavity used in the simulation as the diffuse source room.

Let us consider a rectangular cavity with rigid boundary conditions as sketched in Fig. 3, which intends to simulate a diffuse source room for a two-dimensional analysis. The room dimension $S_x \times S_y$ is chosen as $5\,\mathrm{m} \times 6\,\mathrm{m}$, with an aspect ratio of $2^{1/3}$=1.2 as suggested by Ref. [13]. The window to be tested is mounted on the wall at *x*=5 m, and a sound source *S* is placed near the opposite corner to the test element.

For harmonic analysis conducted in the frequency domain (with time-dependent term $e^{j\omega t}$ being omitted), the Helmholtz equation governing the sound pressure distribution can be written as:

$$\nabla^2 p_c(x,y) + k^2 p_c(x,y) = q e^{j\varphi} \delta(x_s, y_s), \tag{1}$$

where p_c is the sound pressure at any point inside the cavity, *k* is the wavenumber with $k = \omega / c_0$, ω and c_0 are the angular frequency and the sound speed in air, respectively. $j = \sqrt{-1}$ and *t* is time. The air absorption effect can be accounted by using a complex sound speed $c_0\sqrt{1+\eta j}$, with η being the damping loss factor. For the source term, *q* describes the source amplitude and φ the phase angle; δ is the Dirac delta and coordinates (x_s, y_s) specify the source location.

Using the modal expansion approach, the pressure field can be decomposed as:

$$p_c(x,y) = \sum_m a_c^m \varphi_c^m(x,y), \tag{2}$$

where a_c^m is the *m*-th modal amplitude of the cavity; φ_c^m is the mode shape function. For the rigid rectangular-shaped cavity, the following analytical expression for the acoustic modes can be applied:

$$\varphi_c^m = \cos(k_x x)\cos(k_y y) = \cos(\frac{m_x \pi}{S_x} x)\cos(\frac{m_y \pi}{S_y} y), \quad m_x, m_y = 0, 1, 2\cdots, \tag{3}$$

where k_x and k_y are the wavenumbers in the *x* and *y* directions, S_x and S_y are the cavity dimensions, while m_x and m_y are the modal indices, respectively. The resonant frequencies are $f_m = c_0\sqrt{\left(m_x / S_x\right)^2 + \left(m_y / S_y\right)^2}\,/\,2$. Note that the mode shape function for a complex-shaped cavity can be obtained by using FEM [24].

Aiming at a diffuse condition, it is well known that adequate diffuseness is more likely to establish with higher modal density. The modal density can be described by the number of acoustic modes N_{modes} presented in each frequency band. For the present room dimension, the numbers of modes N_{modes} versus the center frequency of 1/3 octave bands from 63 Hz to 2000 Hz are tabulated in Table I. Nelisse and Nicolas [21] suggested a criterion that at least 6 modes shall exist per 1/3 octave band for the diffuse field to form, which corresponds to 125 Hz in Table I. This criterion is further tested by checking the spatial uniformity of sound pressure field within the cavity.

Table I. Number of acoustic modes N_{modes} versus the center frequency of 1/3 octave bands from 63 Hz to 2000 Hz

f_c	N_{modes}	f_c	N_{modes}	f_c	N_{modes}	f_c	N_{modes}
63 Hz	3	160 Hz	12	400 Hz	62	1000 Hz	384
80 Hz	3	200 Hz	16	500 Hz	95	1250 Hz	611
100 Hz	4	250 Hz	24	630 Hz	155	1600 Hz	962
125 Hz	7	315 Hz	44	800 Hz	247	2000 Hz	1523

For the cavity domain S_c with a surrounding boundary B_c, Green's formulation which links the pressure field and boundary conditions can be written as:

$$\int_{S_c} (p_c \nabla^2 \varphi_c^m - \varphi_c^m \nabla^2 p_c) dS_c = \int_{B_c} (p_c \frac{\partial \varphi_c^m}{\partial n} - \varphi_c^m \frac{\partial p_c}{\partial n}) dB_c \,, \tag{4}$$

where the right-hand side of Eq. (4) becomes null for rigid wall surfaces. On inserting Eq. (2) into Eq. (4) and further making use of the modal orthogonal property, one has:

$$a_c^m N_c^m (k^2 - k_m^2) = \int_{S_c} q e^{j\varphi} \varphi_c^m \delta(x_s, y_s) dS_c = q e^{j\varphi} \cos(k_x x_s) \cos(k_y y_s), \tag{5}$$

where $k_m = \sqrt{k_x^2 + k_y^2}$, the source term can be defined as $Q = q e^{j\varphi} \cos(k_x x_s) \cos(k_y y_s)$, and the cavity modal mass is:

$$N_c^m = \int_{S_c} \varphi_c^m \varphi_c^m dS_c = \begin{cases} S_x S_y, & m_x, m_y = 0 \\ 0.5 S_x S_y, & m_x = 0, m_y \neq 0 \text{ or } m_x \neq 0, m_y = 0 \\ 0.25 S_x S_y, & m_x \neq 0, m_y \neq 0 \end{cases}. \tag{6}$$

On substituting the expression of a_c^m into Eq. (2), the sound pressure becomes:

$$p_c = \sum_m Q \varphi_c^m / \left[N_c^m (k^2 - k_m^2) \right]. \tag{7}$$

The *root-mean-square* value of the sound pressure level (SPL) L_r at any receiving point *r* inside the cavity is:

$$L_r(x_r, y_r) = 20 \log(p_{rms} / p_0) = 20 \log \left[\sum_m a_c^m \varphi_c^m (x_r, y_r) / \sqrt{2} p_0 \right], \tag{8}$$

where $p_{rms} = p_c / \sqrt{2}$, p_0 is the reference acoustic pressure (i.e. 20 μPa in air). To validate the above formulation, the SPL at a receiving point (2, 3) m is calculated in the linear frequency range from 10 Hz to 500 Hz, which is compared to the result obtained from FEM analysis. The source strength *q* is set as unity and the phase angle is zero. A sufficient number of modes are included in the calculation to ensure a convergent result, and the damping loss factor is taken as $\eta = 0.005$. Figure 4 shows that the results from the theory and FEM agree perfectly, thus validating the two models.

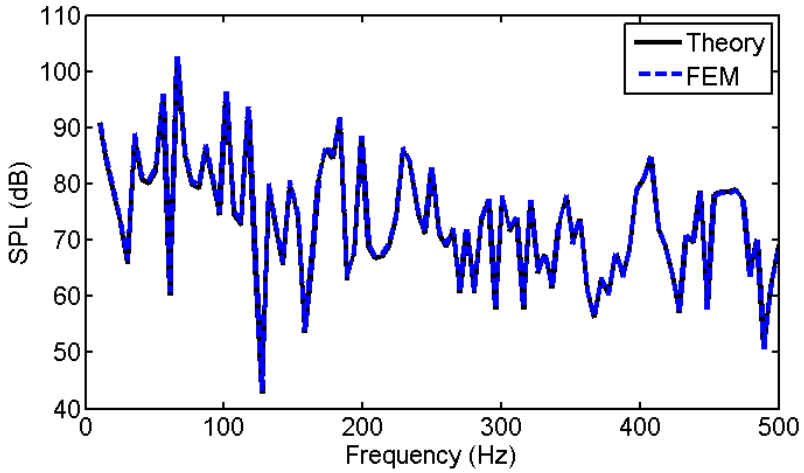

Fig. 4. Comparison of SPLs at the receiving point, predicted using the theoretical formulation and FEM.

To check the pressure field uniformity, the standard deviation of the SPLs within a receiving region is quantified. In the calculation, the entire frequency range of interest is either linearly or logarithmically partitioned into a number of frequency points. To compare the result in the 1/3 octave band, the SPL is averaged over N_f discrete frequencies for each band:

$$L_r(f_c) = \sum_{f=f_l}^{f_u} L_r(f) / N_f , \tag{9}$$

where f_l is the lower-limit, f_u is the upper-limit, f_c is the center frequency of a 1/3 octave band. In Fig. 3, the rectangle shaded in grey color is selected as the receiving region, whose bottom-left and top-right corners are specified at (3, 2) m and (4, 4) m, respectively. A separation distance of 0.2 m in both *x*- and *y*-directions is chosen to sample the receiving points. Using Eq. (9), the SPLs at a total number of $N_r = 66$ points lying in the area are calculated, and their mean value is:

$$\overline{L_r}(f_c) = \sum_{1}^{N_r} L_r(f_c) / N_r . \tag{10}$$

The standard deviation can be calculated as:

$$SD(f_c) = \sqrt{\sum_{1}^{N_r} \left[L_r(f_c) - \overline{L_r}(f_c) \right]^2 / N_r} \ . \tag{11}$$

As discussed in Ref. [13] and [21] , a standard deviation of less than 1.5 dB would be able to support a diffuse field. To verify this for 125 Hz, the standard deviation versus 1/3 octave frequencies is calculated for two cases with $\eta = 0$ and $\eta = 0.005$, respectively. Figure 5 shows that the standard deviation is initially high between 63 Hz and 125 Hz, indicating that the room model is not diffuse in the low-frequency region. Above 125 Hz, the deviation gradually decreases as frequency increases, and the value stabilizes at below 1.5 dB after 250 Hz where the modal density has increased to 24 modes per 1/3 band. Therefore, without further tuning the cavity dimension, the room model is diffuse in the frequency range between 250 Hz and 2000 Hz, and is reasonable diffuse between 125 Hz and 250 Hz.

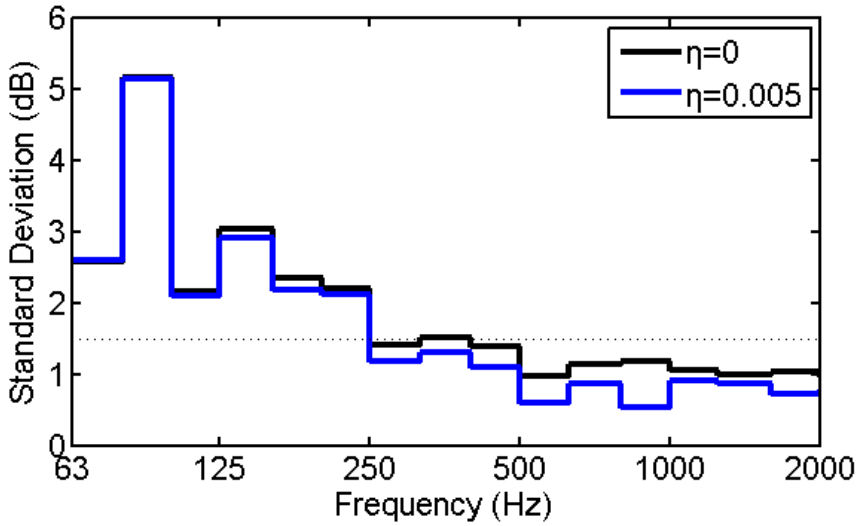

Fig. 5. Standard deviation of the SPLs at the sampled receiving points in Fig. 3.

2.2 Sound reduction index (SRI)

The above source room is used to predict the SRI of the ventilation windows, and the transmitted power is evaluated from the sound radiation into a semi-infinite free space, mimicing a anchoic room, as illustrated in Fig. 6. The SRI can be evaluated by:

$$\mathrm{SRI} = 10\log_{10}(W_S / W_R) = L_S^W - L_R^W, \tag{12}$$

where W_S and W_R are the sound powers; L_S^W and L_R^W the sound power levels (SWLs), being incident on and radiated by the test element, respectively. The semi-infinite free space is realized by embedding the outlet opening in a large sized rigid baffle, with non-reflecting conditions being applied at the far field boundaries.

Given a diffuse source condition, the incident SWL L_S^W can be determined from the averaged SPL in the 2D source room [17]:

$$L_S^W(f_c) = 10\log\left[\frac{A}{2\rho_0 c_0}\left(\frac{\sum 10^{L_S/10}}{N_S}\right)\right], \tag{13}$$

where L_S are the SPLs at N_S measurement points being sampled in the source room, A is the surface area of the test window specimen, ρ_0 is the air density. According to Fig. 6, the above average is taken over the receiving region as specified in Sec. 2.1.

On the other side of the window, non-reflecting radiation boundary is applied to a semicircle. The transmitted SWL can be evaluated by integrating the radiated sound power along the semicircle as:

$$L_R^W(f_c) = 10\log\left[\frac{\int 10^{L_R/10} dr}{(\rho_0 c_0)}\right], \tag{14}$$

where L_R are the SPLs at the radiation boundary. Note that the receiving side can be also simulated using another reverberant room with rigid boundary conditions. Correspondingly, the SRI can be calculated from the difference between the averaged sound pressure levels in the source and receiving room.

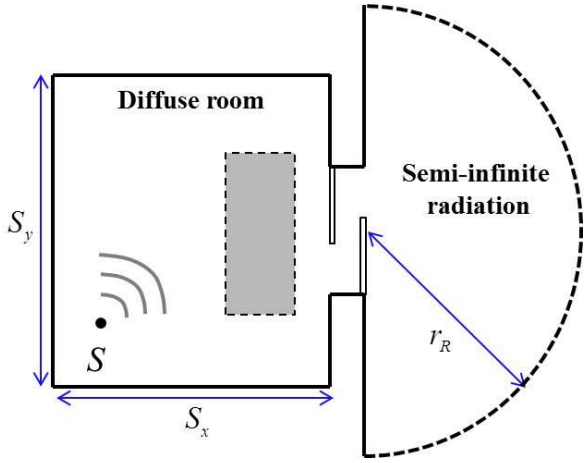

Fig. 6. Prediction of the ventilation window SRI using a numerical model.

To facilitate the calculation, acoustic module under commercial FEM solver COMSOL is used. The source room walls and the window panels are taken as rigid boundaries. A cylindrical radiation boundary is applied to the semicircle, with a radius of r_R = 4m, centrally located at the midpoint of the outlet opening. The mesh criterion requires at least six nodes per wavelength, which is determined by the maximum frequency targeted in the calculation. Considering the valid range of the diffuse room model (as discussed in Sec. 2.1), the frequency spectrum of typical environmental noises and the high computational cost of using FEM for high frequencies, the calculation frequency range is set between 125 Hz to 2000 Hz, consisting of 13 one-third octave bands in total. Within each 1/3 octave band, N_f =30 frequency points are logarithmically partitioned. Further increasing this number has been tested which does not show noticeable influence on the result. In a typical 2D simulation, the

entire calculation domain has roughly 6×10^5 degrees of freedoms, and the computational time is around 4 hours performed on a workstation with two Intel E5450 processors (3 GHz each) and 32 GB RAM. The sound pressure result from the FEM solver is post-processed in MATLAB to obtain the SRI.

2.3 Micro-perforated panel (MPP) absorber

As shown in Fig. 2(c), an open double glazing incorporating a MPP absorber is considered for its possible acoustic benefit. MPPs have been known to be an efficient sound absorber whose *in-situ* absorption greatly dependents on its designing parameters and surrounding environment [23, 25]. The perforation parameters including the diameter of the perforations *d*, panel thickness *t* and perforation ratio σ determine the specific acoustic impedance of a MPP, which can be analytically described by:

$$z_{mpp}=\frac{32\mu t}{\rho_0 c_0 \sigma d^2}\left[(1+\frac{\gamma^2}{32})^{1/2}+\frac{\sqrt{2}}{32}k\frac{d}{t}\right]+\frac{j\omega t}{c_0\sigma}\left[1+(9+\frac{\gamma^2}{2})^{-1/2}+0.85\frac{d}{t}\right], \quad (15)$$

where μ is the air viscosity, γ is the perforation constant $\gamma=d\sqrt{\rho_0\omega/4\mu}$.

As a resonant absorber, the MPP impedance together with the size of the backing cavity controls the effective frequency for sound absorption. The locally-reactive absorption coefficient of a MPP absorber under normal incidence condition (e.g., impedance tube) is:

$$\alpha=\frac{4\,\mathrm{Re}(z_{mpp})}{[\mathrm{Re}(z_{mpp})+1]^2+[\mathrm{Im}(z_{mpp})-\cot(kD)]} \quad (16)$$

where *D* is the backing cavity depth.

To verify the above formula which will be later incorporated into the numerical model, a MPP absorber sample is fabricated and analyzed for its acoustic characteristics. Fig. 7(a) shows the metal MPP fabricated by chemical etching technology, in which the hole size (0.23 mm) and the panel thickness (0.2 mm) are much smaller compared with the ones used by Kang *et al.* [3]. This helps to increase the MPP resistant part for a superior sound absorption performance and a wider absorption bandwidth [25]. As shown in Fig. 7(b) for two backing cavity depths D=5 cm and D=3 cm, the predicted absorption coefficient α curves and the measured ones from the impedance tube are presented, showing excellent agreement. This implies the validity of Eq. (15) with very small holes. Note that if daylighting is required, MPP can be fabricated based on transparent material or even membranes.

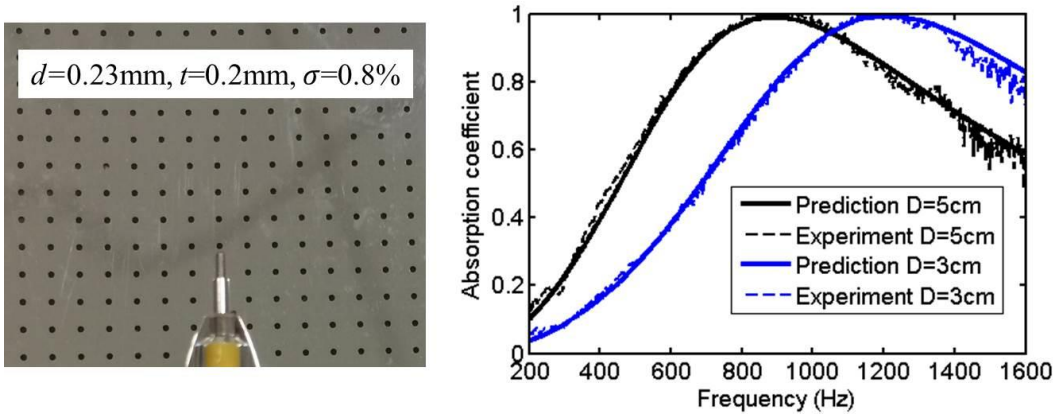

Fig. 7. a) A MPP sample fabricated by chemical etching technology; b) comparison of the predicted absorption coefficients and measured ones from the impedance tube test.

3. Results and discussions

The SRI characteristics of various ventilation windows as shown in Fig. 2 are analyzed using the proposed numerical model. 2D simulations are conducted to save

the computational cost. As shown in Fig. 8, an aperture on the wall between a source and a receiving field has a fixed total height of H=1.5 m, where an open single glazing is mounted with an adjustable opening size O. The SRIs for four opening sizes are simulated and presented in Fig. 8, showing relatively smooth responses. It can be seen that when O=1.5 m, the predicted SRI varies around zero along the frequency, indicating that a full opening is nearly transparent to sound. With smaller opening sizes, the SRI curves are in similar trend but with higher values. Since the diffuse source room intends to provide a uniformly distributed incident field, it would be reasonable to assume the sound intensity impinging on the test specimen is nearly uniform. Hence, the transmitted power would be proportional to the area ratio between the opening and the total window height, i.e., O/H. This allows an estimation of open single glazing SRI by simply considering the geometric factor:

$$\mathrm{SRI}=10\log(H/O)\,. \tag{17}$$

When decreasing the opening size from 0.75 m to 0.3 m, the above formula suggests a SRI of 3 dB for a half-open window (O=0.75 m), 4.8 dB for a 1/3-open window (O=0.5 m) and 7 dB for a 1/5-open (O=0.3 m) window. In Fig. 8, these estimated values show good correlations with the predicted SRI curves. It is also noted that the insulation of a single glazing is relatively low. To maintain a SRI of minimum 10 dB, the window area that is allowed to open should be less than 1/10.

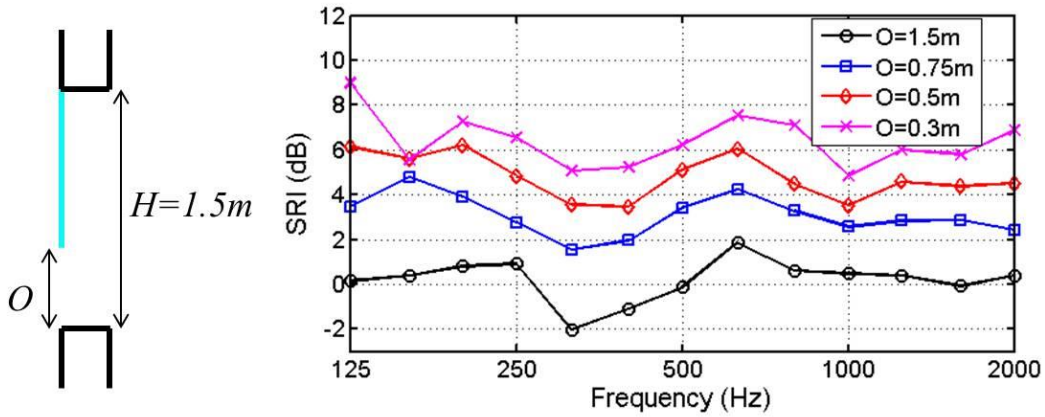

Fig. 8. Sound reduction index of an open single glazing with adjustable opening size *O* in one-third octave band.

To improve the sound insulation, a second layer separated by a distance of *W* is added to form an open double glazing as illustrated in Fig. 9, with an acoustic cavity formed between the double glazing. The staggered openings have an identical size *O*. The impedance mismatch at the inlet-outlet, as well as the cavity resonance effect makes the double glazing essentially like a duct silencer. Part of the incident energy is reflected back to the source domain in order to achieve sound attenuation. In Fig. 9, the spacing *W* is first set as 0.3 m and the effect of varying opening size is studied. It is seen that the SRI of the open double glazing shows resonant behavior in the low-to-mid frequencies, whereas the mid-to-high frequency response is rather flattened. As expected, a smaller opening size generally leads to a higher SRI. It is understandable that the cavity resonance effect is more significant at low frequencies, due to the modal coupling between the cavity and the inlet-outlet domain. This suggests that the low-to-mid frequency region is mainly resonance-controlled. As to the flattened SRI at higher frequencies, the formula in Eq. (17) can be extended to estimate the effect of a double glazing by only considering the geometrical factor. By

assuming that the sound power entering through the inlet opening is sufficiently redistributed and thus the energy density is also uniform in the cavity, the ratio between the incident sound power from the source and transmitted power is O^2/H^2, leading to an estimated SRI of:

$$\text{SRI}=10\log(H/O)^2 = 20\log(H/O)\,. \tag{18}$$

Intuitively, the validity of this assumption would be above the cut-off frequency of the duct, formed between the double glazing with a width of *W*. This frequency limit is 560 Hz for *W*=0.3 m. As seen in Fig. 9, the predicted SRI responses for the three opening sizes in the flattened region correlate well with the estimated values starting from 500 Hz, suggesting a primarily geometry-controlled effect.

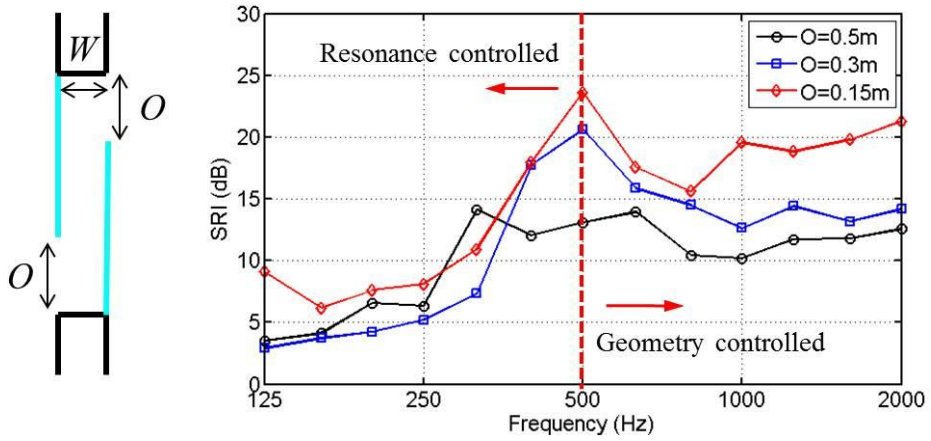

Fig. 9. Sound reduction index of open double glazing with adjustable opening size *O*, the spacing between glazing is *W*=0.3 m.

For both open single and double glazing, the estimated SRIs versus decreasing opening size *O*, predicted using Eq. (17) & (18), respectively, are plotted in Fig. 10. It is seen that reducing the opening gradually results in higher noise reduction, and this trend is more obvious with open double glazing. In addition, Fig. 11 depicts the variation of SRI with different spacing *W* (depth of the cavity), where the opening size

is kept as O=0.5 m. The general trend is that larger spacing performs better at lower frequencies, although the difference is not distinct. While at high frequencies, the three curves show similar SRI of 10 dB, in agreement with Eq. (18).

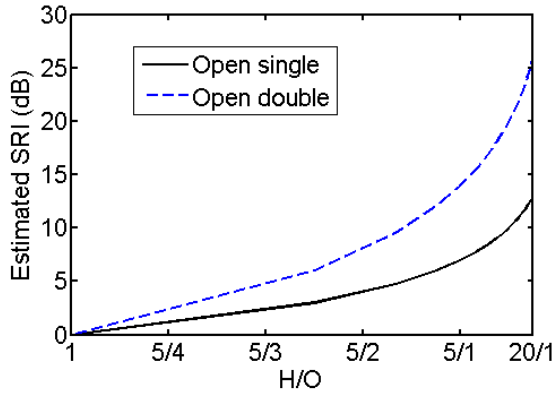

Fig. 10. Trend of estimated SRI for both open single and double glazing versus decreasing open size O.

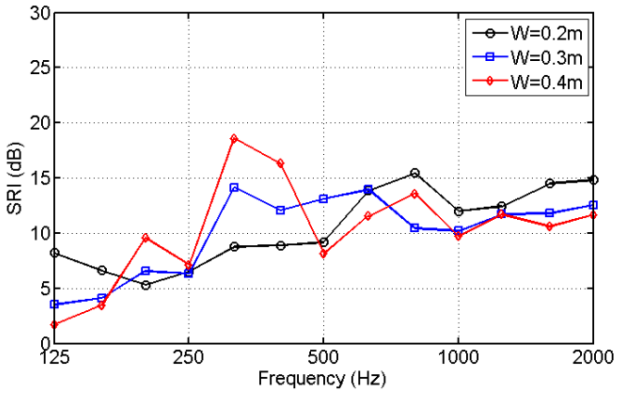

Fig. 11. Sound reduction index of open double glazing with varying spacing, opening size O=0.5 m.

The MPP absorber as discussed in Sec. 2.3 is incorporated into the open double glazing. The perforation parameters are d=0.23 mm, t=0.2 mm, $\sigma = 0.8\%$, and the double glazing with O=0.5 m and W=0.3 m is taken as benchmark for comparisons. The cavity backing the MPP is partitioned with honeycomb structures. With D=0.05 m, Fig. 12 presents a comparison between the open single glazing, open double

glazing with and without MPP absorber, with O/H being kept as 1/3. From 315 Hz to 2000 Hz, the SRI of the open single glazing is low with a mean value of 5 dB, which increases to 10 dB with the open double glazing. Adding MPP absorber shows a significant improvement, as evidenced by a flattened SRI reaching as high as 20 dB. By simply using a term α_w to describe the percentage of sound energy absorbed by the MPP in the cavity, Eq. (18) can be extended to tentatively explain this effect:

$$\text{SRI}=20\log(H/O)-10\log(1-\alpha_w)\,, \tag{19}$$

where α_w depends on a number of factors such as the MPP absorption coefficient α, the double glazing orientation, the size and location of the MPP, etc.

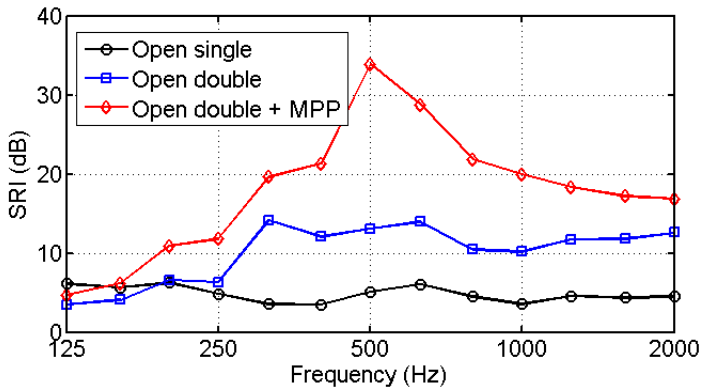

Fig. 12. Comparison of sound reduction indices of open single glazing (O=0.5 m), open double glazing (O=0.5 m, W=0.3 m), and open double glazing with MPP absorber (d=0.23 mm, t=0.2 mm, $\sigma=0.8\%$, D= 0.05m).

The depth D of the backing cavity behind MPP can be varied to control the effective frequencies. Figure 13 shows the SRI results for three cavity depths with D=0.03 m, 0.05 m and 0.1 m, where the corresponding α curves calculated using Eq. (16) are appended. With a larger depth value, the sound attenuation is more effective at lower frequencies, as expected. The SRI comparison also shows the possibility of

achieving an optimized performance in a prescribed frequency range by tuning the system parameters.

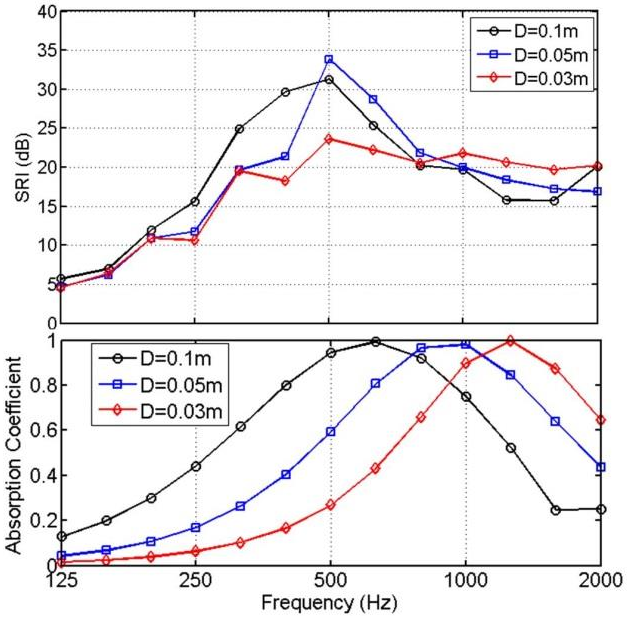

Fig. 13. (a) Sound reduction indices of open double glazing with MPP absorber, the depth *D* of the cavity backing MPP is varied. (b) The corresponding MPP absorption coefficients under normal incidence condition, calculated using Eq. (16).

As an experimental validation, the proposed numerical model is used to evaluate the sound insulation of several ventilation windows tested in an experimental study [7, 8]. As shown in Fig. 14, four typical window configurations were selected from the measurement report, namely: a) a standard top-hung window (open single glazing) with a height of 1.49 m; (b) an open double glazing with a height of 1.49 m; (c) a larger open double glazing (height 2.38 m); and (d) a double glazing treated with sound absorbing material on the glass and frame (height 2.38 m). The window is opened through sashes, where the size of the openings is kept as 0.3 m for all cases, as shown in Fig. 14. The 3D windows can be considered as extrusions from the

corresponding 2D cross-sections, with a window width of 1.2 m. 2D model is used to simulate a cross-section of the window. The SRI measurement was conducted according to ISO10140, with a reverberant source room of size 120 m^3 and a receiving room size of 60 m^3 [8].

In Fig. 15, the predicted SRIs using the proposed model for cases E1 to E2, and the experimental SRIs from the reference report are compared, showing generally good agreements. The discrepancies are less than 2 dB, which may be affected by various reasons such as experimental variability, geometry uncertainty, unknown air damping, flanking transmission, etc. The overall prediction accuracy is acceptable. The lowest black curve corresponds to SRI of the top-hung window E1 [Fig. 14(a)]. With an opening size of 0.3 m, i.e., 1/5 of the total window height, the SRI value is about 7~8 dB, matching with Eq. (17). The double-glazing window E2 [Fig. 14(b)] doubles the SRI to 15 dB at frequencies above 600 Hz, and the resonance effect at lower frequencies attributed to the cavity longitudinal mode is seen. The third case E3 [Fig. 14(c)] increases the height of the double-glazing window, reducing the opening area to 1/8 of the total height. The resultant SRI seems like a parallel transport of E2 SRI with an increment of 3 dB. For case E4, porous sound absorbing material is added onto the window glass and frame. The thickness of the absorber is 0.04 m and 0.02 m on the two window glasses, and 0.02 m on the frame enclosing the cavity. The simulation model treats the absorber as a homogenous acoustic domain using the simplest Delany-Bazley model, where the flow resistivity is assumed as 50000 $Pa.s/m^2$. The SRI shows a distinct improvement compared with the previous three

cases with rigid surfaces. The effectiveness of using internal sound absorber to enhance the sound insulation of an open double glazing is clearly demonstrated.

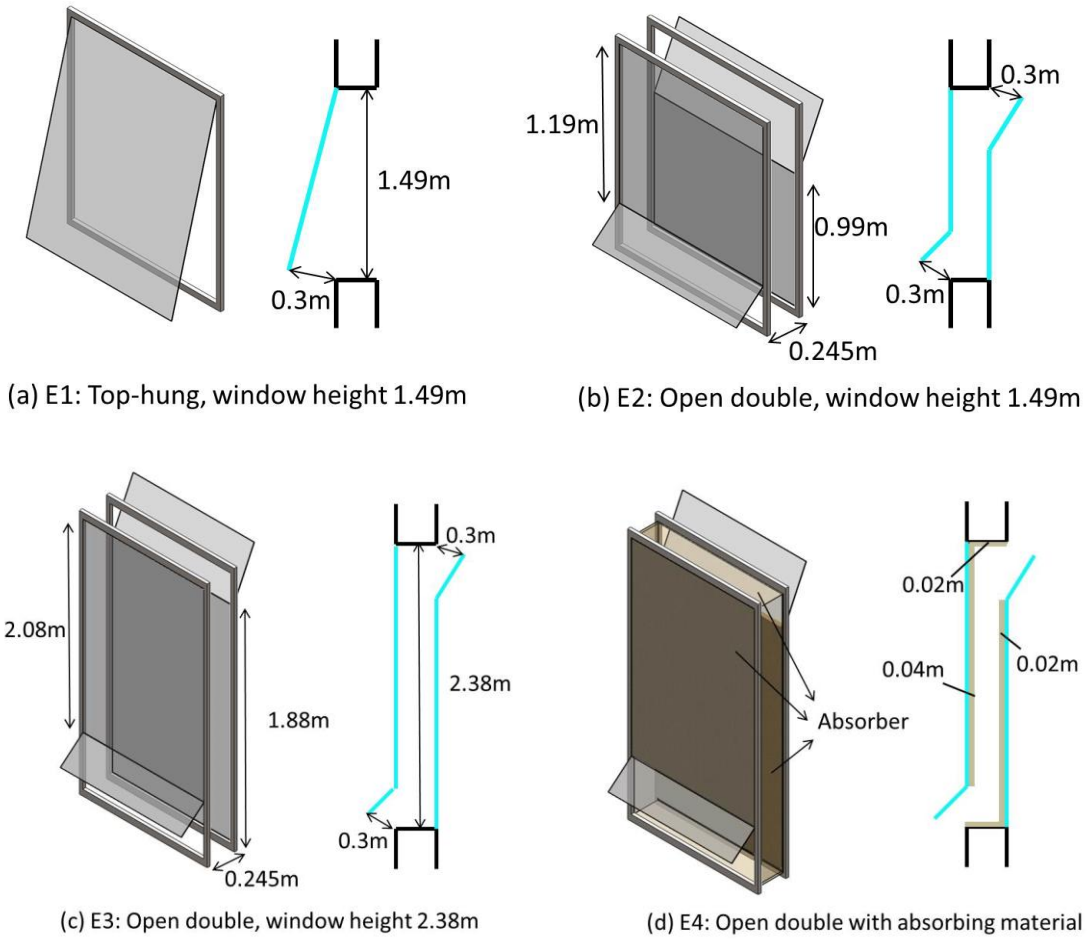

Fig. 14. Configurations of four validation cases: a) standard top-hung window; (b) open double glazing, height 1.49 m; (c) open double glazing, height 2.38 m; and (d) open double glazing treated with sound absorbing material on the glass and frame.

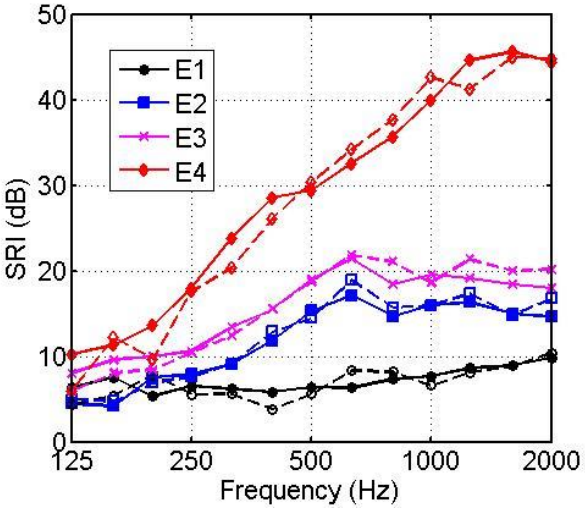

Fig. 15. Experimental validation of the simulation model: the solid lines are experimental results and the corresponding dashed lines are simulated results.

4. Conclusions

To numerically evaluate the sound insulation of ventilation windows, a simulation model which complies with the recommendations in the ISO standard has been proposed. The model consists of an acoustic cavity with rigid boundaries on the source side to provide a diffuse field condition, and a free field radiation with an infinite baffle at the receiver side. To ensure adequate diffuseness, the uniformity of the pressure field within the source room has been verified using a proposed theoretical model. Examinations on the distribution of room modes and standard deviation of SPLs indicate that the source field has reasonable diffuseness in the interested frequency range from 125 Hz to 2000 Hz.

Simulations using the proposed model have been carried out to investigate the SRI characteristics of some typical ventilation window configurations. From the numerical results, a partially open single glazing is shown to exhibit a smooth SRI response in

the entire frequency range. The insulation is rather low and marginally acceptable for practical noise control. By adding a second layer, the open double glazing with staggered openings shows an improved sound insulation with the same opening size. Results suggest that the SRI of the double glazing is mainly controlled by the cavity resonance effect in the low-to-mid frequency range, which transits into a geometry-controlled region at higher frequencies, featuring a flattened SRI response. As to the effect of varying the opening size, two simple formulas have been suggested to estimate the SRI of both open single- and double-glazing, which can be used to guide the practical design of ventilation windows.

To illustrate the acoustic benefit of adding sound absorbers into the cavity between the double glazing, a MPP has been incorporated into the simulation model, with its characteristics being verified using a fabricated sample. Placing a MPP with a honeycomb backing cavity in front of the second glazing allows achieving a moderate SRI of roughly 20 dB in the frequencies above 250 Hz. This value was 10 dB higher than its counterpart without MPP, and 15 dB higher than the open single glazing. Such window design can sought as a promising product by properly choosing the window and absorber parameters, where the proposed numerical tool can be exploited to effectively tune the system parameters.

Acknowledgements

This material is based on research/work supported by the Singapore Ministry of National Development and National Research Foundation under L2 NIC award No. L2NICCFP1-2013-9.

REFERENCES

[1] R. Ford, G. Kerry, The sound insulation of partially open double glazing, Applied Acoustics, 6 (1973) 57-72.

[2] G. Kerry, R.D. Ford, The field performance of partially open dual glazing, Applied Acoustics, 7 (1974) 213-227.

[3] J. Kang, M.W. Brocklesby, Feasibility of applying micro-perforated absorbers in acoustic window systems, Applied Acoustics, 66 (2005) 669-689.

[4] J. Kang, Z. Li, Numerical Simulation of an Acoustic Window System Using Finite Element Method, Acta Acustica united with Acustica, 93 (2007) 152-163.

[5] H. Huang, X. Qiu, J. Kang, Active noise attenuation in ventilation windows, The Journal of the Acoustical Society of America, 130 (2011) 176-188.

[6] N. Yuya, N. Sohei, N. Tsuyoshi, Y. Takashi, Sound propagation in soundproofing casement windows, Applied Acoustics, 70 (2009) 1160-1167.

[7] L.S. Søndergaard, H.S. Olesen, Investigation of sound insulation for a Supply Air Window, Forum Acusticum 2011, Denmark.

[8] L.S. Søndergaard, H.S. Olesen, Lydmæssig optimering af Russervinduer (Acoustical optimization of Supply Air Windows), Environmental project No. 1417, Page 17-60 (2012).

[9] Y.G. Tong, S.K. Tang, Plenum window insertion loss in the presence of a line source—A scale model study, The Journal of the Acoustical Society of America, 133 (2013) 1458-1467.

[10] Y.G. Tong, S.K. Tang, J. Kang, A. Fung, M.K.L. Yeung, Full scale field study of

sound transmission across plenum windows, Applied Acoustics, 89 (2015) 244-253.

[11] X. Yu, F.S. Cui, L. Cheng, On the acoustic analysis and optimization of ducted ventilation systems using a sub-structuring approach, The Journal of the Acoustical Society of America, 139 (2016) 279-289.

[12] ISO, 10140 Acoustics, Laboratory measurement of sound insulation of building elements.

[13] C.I. Papadopoulos, Development of an optimised, standard-compliant procedure to calculate sound transmission loss: design of transmission rooms, Applied Acoustics, 63 (2002) 1003-1029.

[14] C.I. Papadopoulos, Development of an optimised, standard-compliant procedure to calculate sound transmission loss: numerical measurements, Applied Acoustics, 64 (2003) 1069-1085.

[15] J.-D. Chazot, J.-L. Guyader, Prediction of transmission loss of double panels with a patch-mobility method, The Journal of the Acoustical Society of America, 121 (2007) 267-278.

[16] A. Arjunan, C.J. Wang, K. Yahiaoui, D.J. Mynors, T. Morgan, V.B. Nguyen, M. English, Development of a 3D finite element acoustic model to predict the sound reduction index of stud based double-leaf walls, Journal of Sound and Vibration, 333 (2014) 6140-6155.

[17] A. Dijckmans, G. Vermeir, Numerical Investigation of the Repeatability and Reproducibility of Laboratory Sound Insulation Measurements, Acta Acustica united with Acustica, 99 (2013) 421-432.

[18] J. Poblet-Puig, A. Rodríguez-Ferran, Modal-based prediction of sound transmission through slits and openings between rooms, Journal of Sound and Vibration, 332 (2013) 1265-1287.

[19] C. Díaz-Cereceda, J. Poblet-Puig, A. Rodríguez-Ferran, The finite layer method for modelling the sound transmission through double walls, Journal of Sound and Vibration, 331 (2012) 4884-4900.

[20] C.M. Mak, Z. Wang, Recent advances in building acoustics: An overview of prediction methods and their applications, Building and Environment, 91 (2015) 118-126.

[21] H. Nélisse, J. Nicolas, Characterization of a diffuse field in a reverberant room, The Journal of the Acoustical Society of America, 101 (1997) 3517-3524.

[22] R. Tomiku, T. Otsuru, Y. Takahashi, Finite Element Sound Field Analysis of Diffuseness in Reverberation Rooms, Journal of Asian Architecture and Building Engineering, 1 (2002) 2_33-39.

[23] C. Yang, L. Cheng, Sound absorption of microperforated panels inside compact acoustic enclosures, Journal of Sound and Vibration, 360 (2016) 140-155.

[24] N. Totaro, J.L. Guyader, Efficient positioning of absorbing material in complex systems by using the Patch Transfer Function method, Journal of Sound and Vibration, 331 (2012) 3130-3143.

[25] X. Yu, L. Cheng, X. You, Hybrid silencers with micro-perforated panels and internal partitions, The Journal of the Acoustical Society of America, 137 (2015) 951-962.

Figure captions

Fig. 1. Experimental evaluation of the SRI of a window, as specified by ISO 10140.

Fig. 2. (a) Open single glazing; (b) Open double glazing, the inlet-outlet openings are staggered; (c) Open double glazing with sound absorber, e.g., honeycomb MPP.

Fig. 3. A rectangular cavity used in the simulation as the diffuse source room.

Fig. 4. Comparison of SPLs at the receiving point, predicted using the theoretical formulation and FEM.

Fig. 5. Standard deviation of the SPLs at the sampled receiving points in Fig. 3.

Fig. 6. Prediction of the ventilation window SRI using a numerical model.

Fig. 7. a) A MPP sample fabricated by chemical etching technology; b) comparison of the predicted absorption coefficients and measured ones from the impedance tube test.

Fig. 8. Sound reduction index of an open single glazing with adjustable opening size O in one-third octave band.

Fig. 9. Sound reduction index of open double glazing with adjustable opening size O, the spacing between glazing is W=0.3 m.

Fig. 10. Trend of estimated SRI for both open single and double glazing versus decreasing open size O.

Fig. 11. Sound reduction index of open double glazing with varying spacing, opening size O=0.5 m.

Fig. 12. Comparison of sound reduction indices of open single glazing (O=0.5 m), open double glazing (O=0.5 m, W=0.3 m), and open double glazing with MPP absorber (d=0.23 mm, t=0.2 mm, $\sigma = 0.8\%$, D= 0.05m).

Fig. 13. (a) Sound reduction indices of open double glazing with MPP absorber, the depth D of the cavity backing MPP is varied. (b) The corresponding MPP absorption coefficients under normal incidence condition, calculated using Eq. (16).

Fig. 14. Configurations of four validation cases: a) standard top-hung window; (b) open double glazing, height 1.49 m; (c) open double glazing, height 2.38 m; and (d) open double glazing treated with sound absorbing material on the glass and frame.

Fig. 15. Experimental validation of the simulation model: the solid lines are experimental results and the corresponding dashed lines are simulated results.

Table caption

Table I. Number of acoustic modes N_{modes} versus the center frequency of 1/3 octave bands from 63 Hz to 2000 Hz